Check for updates

Formation of a Key Intermediate Complex Species in Catalytic Hydrolysis of NH₃BH₃ by Bimetal Clusters: Metal-Dihydride and Boron-Multihydroxy

W. J. Yan [1,2], Y. F. Zheng [1], T. W. Zhou [1], G. Z. Wang [3*], D. D. Wang [1] and H. K. Yuan [1*]

[1] School of Physical Science and Technology, Southwest University, Chongqing, China, [2] School of Mechatronics and Information Engineering, Chongqing College of Humanities, Science & Technology, Chongqing, China, [3] School of Electronic Information Engineering, Yangtze Normal University, Chongqing, China

The hydrolysis of AB (AB, NH₃BH₃) with the help of transition metal catalysts has been identified as one of the promising strategies for the dehydrogenation in numerous experiments. Although great progress has been achieved in experiments, evaluation of the B-N bond cleavage channel as well as the hydrogen transfer channel has not been performed to gain a deep understanding of the kinetic route. Based on the density functional theory (DFT) calculation, we presented a clear mechanistic study on the hydrolytic reaction of AB by choosing the smallest NiCu cluster as a catalyst model. Two attacking types of water molecules were considered for the hydrolytic reaction of AB: stepwise and simultaneous adsorption on the catalyst. The Ni and Cu metal atoms play the distinctive roles in catalytic activity, i.e., Ni atom takes reactions for the H_2O decomposition with the formation of $[OH]^-$ group whereas Cu atom takes reactions for the hydride transfer with the formation of metal-dihydride complex. The formation of Cu-dihydride and B-multihydroxy complex is the prerequisite for the effectively hydrolytic dehydrogenation of AB. By analyzing the maximum barrier height of the pathways which determines the kinetic rates, we found that the hydride hydrogen transferring rather than the N-B bond breaking is responsible to the experimentally measured activation energy barrier.

Keywords: DMol³, first-principal calculation, bimetal clusters, catalytic, DFT

1. INTRODUCTION

Among many practical hydrogen storage materials, ammonia-borane (AB, NH₃BH₃) is believed to be an attractive solid hydrogen storage candidate owing to its high hydrogen content, nontoxic, excellent solubility, and stability in water (Peng and Chen, 2008; Hamilton et al., 2009; Staubitz et al., 2010; Jiang and Xu, 2011; Sanyal et al., 2011; Thorne et al., 2011; Lu and Xu, 2012; Xi et al., 2012). To enhance the kinetics of the hydrogen release for its on-board applications, intensive efforts have been made in solid state by thermolysis dehydrogenation (Demirci and Miele, 2009; Hamilton et al., 2009) and in solution by hydrolysis and methanolysis dehydrogenation (Xu and Chandra, 2007; Umegaki et al., 2009; Chua et al., 2011). In the absence of suitable catalysts, the

thermal/hydrolytic decomposition to generate the hydrogen is a very slow process and it has to undergo several step reactions at very high temperature (Hu et al., 1978; Matus et al., 2007; Stowe et al., 2007; Huang and Autrey, 2012), which seriously restricts the development of AB as a promising hydrogen storage material. In the perspective of hydrolysis dehydrogenation, finding high active and low-cost catalysts to make AB completely release its hydrogen under moderate conditions is a key point for this system.

Up to now, there has been a steady growth in a number of publications dealing with the catalytic hydrolysis of AB to generate the hydrogen at low temperature (Jiang and Xu, 2011; Patel and Miotello, 2015). Originally, noble metal catalysts such as Au (Chandra and Xu, 2007), Pt (Chandra and Xu, 2006a, 2007; Mohajeri et al., 2007; Chen et al., 2014), Pd (Chandra and Xu, 2007; Metin et al., 2011; Kılıç et al., 2012), Rh (Chandra and Xu, 2006a, 2007; Zahmakiran and Özkar, 2009; Karahan et al., 2012), Ru (Chandra and Xu, 2007; Rachiero et al., 2011a; Can and Metin, 2012; Liang et al., 2012; Zhou Q. et al., 2016), and Ir (Wang et al., 2017b) were extensively explored, although their expensive costs are the dominate disadvantage for the potential applicability. Along with the development of cheaper catalysts without the loss of highly efficient, nanoparticle based on more abundant first-row transition metals Fe (Xu and Chandra, 2006; Yan J. M. et al., 2008; Dinç et al., 2012), Co (Xu and Chandra, 2006; Demirci and Miele, 2010; Yan et al., 2010b; Metin and Özkar, 2011; Li et al., 2017), Ni (Xu and Chandra, 2006; Kalidindi et al., 2008a; Yan et al., 2009; Metin et al., 2010; Metin and Özkar, 2011; Li et al., 2017; Wang et al., 2017a), and Cu (Xu and Chandra, 2006; Kalidindi et al., 2008a,b; Zahmakiran et al., 2010) have also been tentatively studied, however, they have only moderate catalysis and lack the desiring stability in the hydrolysis conditions. To get over the challenges of cost expensiveness of the noble metal as well as the catalytic limitation of transition metal, the modulation of the noble metal content by alloying with first-row transition metal was considered as a feasible solution, because their active sites could be maintained and their active capabilities could be improved in alloying catalysts. As one expected, most bimetallic catalysts such as Cu(Fe, Ni, Ru) (Rachiero et al., 2011b; Lu et al., 2013, 2014; Zhang et al., 2016), (Pd, Au, Ru)Co (Yan et al., 2010a; Chen et al., 2011; Sun et al., 2011; Lu et al., 2012; Wang et al., 2012), (Au, Ag, Pt, Ru)Ni (Chen et al., 2007, 2012; Yao C. F. et al., 2008; Jiang et al., 2010), and (Ni, Cu)Pd (Çiftci and Metin, 2014; Güngörmez and Metin, 2015) have been reported to exhibit the better performance than the monometal catalysts for the hydrogen generation from the hydrolysis of AB. It was deduced that the formations of the heterometallic bonds can adjust the bonding (molecular) orbitals of catalyst surface atoms to reactant with AB and H_2O molecules. This can stabilize the reaction intermediates and lead to the improvement of catalytic activity on AB for hydrogen generation (Lu et al., 2013). The behind reason is attributed to the synergistic effect between the heterometallic atoms that originates from the electronic effect (such as the adjustment of d-band level or charge transfers) and the structural morphology (such as the formation of core-shell or mixing structures).

By measuring the composition of hydrolytic products in the presence of various transition metal-based catalysts (Yao C. F. et al., 2008; Rachiero et al., 2011b; Chou et al., 2012; Liu et al., 2012; Komova et al., 2016), it was confirmed that 1 mole of AB is hydrolyzed to give nearly 1 mole of NH_4^+ ions and 3 moles of H_2 gas. For example, Yao C. F. et al. (2008) have chemically identified that the gaseous product is exclusively H_2 molecules and the soluble product is NH_4^+ ions. Based on NMR experiment, Rachiero et al. (2011b) have demonstrated that the initial product $B(OH)_4^-$ is adsorbed over the catalyst surface without B-N adducts or intermediates desorbing. Consequently, the overall hydrolysis reaction of AB can be described as $NH_3BH_3 + 3H_2O \xrightarrow{\text{catalyst}} \text{catalyst} \cdot NH_3 + B(OH)_3 + 3H_2 \uparrow$, which was readily confirmed by the composition of reaction products using the x-ray diffraction analysis (Mohajeri et al., 2007; Brockman et al., 2010; Chou et al., 2012; Liu et al., 2012; Komova et al., 2016). The NH_3 and $B(OH)_3$ are being dissolved in water as described by a well known acid-base equilibrium $NH_3 + H_2O \leftrightarrow NH_4^+ + OH^-$ and $B(OH)_3 + OH^- \leftrightarrow B(OH)_4^- \leftrightarrow BO_2^- + 2H_2O$ (Brockman et al., 2010; Komova et al., 2016). These final products suggest that one portion of H_2 molecule is generated through the H-O bond breaking in H_2O and the other is generated through the H-B bond breaking in AB, and NH_3 molecule is formed by B-N bond cleavage. In addition, the observations of these experiments are consistent with the Langmuir-Hinshelwood mechanism for the heterogeneous catalysis (Basu et al., 2010; Rakap and Özkar, 2010), i.e., AB and H_2O adsorb over the catalytic surface to be hydrolyzed upon the formation of the final by-product $B(OH)_4^-$. Although great progress has been achieved in the experiments for the fast and complete H_2 release, evaluations of the B-N bond cleavage channel and the hydrogen transfer channel have not been performed to gain a deep understanding of the kinetic route, to suggest a methodological scheme which properly describes these reactions, and to find out crucial step to tune the reactions for future application in H_2 storage. In our opinion, this is a substantial gap in this field of research.

By using the density functional theory (DFT) calculations, herein, we investigate the reaction pathways of H_2 release from the hydrolytic AB and examine the catalytic roles of small NiCu clusters. Experimentally, NiCu bimetallic nanoparticles have been successfully fabricated and the catalytic activity was evaluated in the hydrolytic dehydrogeneration of AB (Lu et al., 2014; Zhang et al., 2016). The results shown that NiCu bimetallic nanoparticles exhibit the excellent catalytic activity and the low activation energy barriers owning to the charge transfer between Cu and Ni atoms (Lu et al., 2014; Zhang et al., 2016). Since the dehydrogenation reaction of AB involves an ionic recombination of hydridic $H^{\delta-}$ and protic $H^{\delta+}$, the positively Ni atom would play an attractive role to interact with the $[OH]^-$ group by hydrolyzing H_2O while the negatively Cu atom would act as an agent to accept the hydrolyzed H^+ ion. Considering the dissociation of NH_3 molecule from AB in the experiments, we naturally deduce the hydrolytic dehydrogenation of AB that the hydridic H(B) atoms from –BH_3 edge of AB would like to interact with the protic H(O) atoms from H_2O, aggregating and forming

three H$_2$ molecules. Firstly and importantly, validation of the aforementioned rules and trends is crucial and necessary from the electronic structure. Secondly, the potential energy surfaces on the reaction channels describe the heights of activation energy barriers and thermodynamic stabilities, which can be used to compare with the experimental measurement. Finally, our results are important in developing the evidence-based experimental requirements for the safe handling of this hydride in everyday laboratory and industrial practice. In what follows, we will firstly describe the computational methodology used in the work in section 2, and then present our results and discussions in section 3. Finally, a summary is given in section 4.

2. METHODS

Our calculations have been performed by using the Density Functional Theory (DFT) based DMol^3 code (Delley, 2000), where the Perdew-Wang (PW91) exchange-correlation potential (Becke, 1988; Perdew and Wang, 1992) to the generalized gradient approximation (GGA) (White and Bird, 1994) was adopted. The double numerical basis sets with the p-polarization function (DNP), all electrons treated as the valance electrons, and the thermal corrections were employed in the calculations for the equilibrium geometries of all molecular species, i.e., the reactant-complex (R), transition states (TS), intermediates (IM), and products (P). The DNP basis set is quite a bit better than Gaussian 6-31G** basis set under the accurate level, and the former one is more effective than the latter one (Hirshfeld, 1977; Wu et al., 2013). The harmonic vibrational frequencies were determined at the same level to confirm whether the optimized structures are local minima (no imaginary frequency) or transition states (one imaginary frequency) and to evaluate the zero-point vibrational energy. To obtain the TS, linear synchronous transit (LST) and quadratic synchronous transit (QST) methods were firstly utilized to execute an extensive search, and then the TS optimization has been done with the eigenvector-following methods, following which the TS confirmation was performed to produce a refined reaction path based on LST or QST (Peng and Schlegel, 1993; Peng et al., 1996; Ayala and Schlegel, 1997). The convergence criterions were set to 2×10^{-5} Ha for the maximum energy change, 4×10^{-3} Ha/Å for the maximum force, 5×10^{-3} Å for the maximum atomic displacement, respectively. The activation energy barrier (E$_{act}$) determines whether or not the reactions take place spontaneously and reach to the final state without the extra-energy absorbed from the outside. It was calculated as the energy difference between the initial reactants and the highest transition state of a whole reaction pathway, i.e., E$_{act}$ = E$_{HTS}$-E$_{React}$. The energy values hereafter are enthalpy except for specially mentioned. The zero-point energy and enthalpy corrections have not been considered, because the corrections always reduce the values in a small magnitude (Zhou T. et al., 2016).

For free AB, we found that the bond-lengths of B-N, B-H, and N-H bonds are 1.66, 1.22, 1.02 Å, respectively, which are in good agreement with the experimental measurements (Thorne et al., 2011) and theoretical values under more precise calculations

(Gaussian-B3LYP/6-311+g*) (Zhou T. et al., 2016). Thus, we have a high degree of confidence in our structural configurations. To validate our method in calculating the dehydrogenation dynamics, we have calculated the dehydrogenation pathways of AB without (**Figures 1A,B**) and with (**Figures 1C,D**) the help of Cu$_2$ catalyst by using the DMol^3 and Gaussian methods. From **Figure 1**, we noted that the DMol^3 method (BPW91/DNP) gives a similar variational trend as the Gaussian method does (Zhou T. et al., 2016). Although the IM states and TS states under the former calculations are higher in energy than under the latter calculations, both methods report the same energy orderings of these states. Typically, the highest energy barrier (the decisive reaction step) (1.953 eV) and the exoergic energy (0.162 eV) of the whole reaction path are well reproduced by DMol^3 method. Furthermore, the Van der Waals correction (Bučko et al., 2010) has been taken into account (BPW91/DNP/OBS) for the benchmark calculations, however, the results (red lines) shown that it does not present the superiority. Therefore, the following calculations were performed within the DMol-BPW91/DNP method.

3. RESULTS

3.1. Synergistic Adsorption of H$_2$O and AB Molecules on NiCu Dimer

The initial interactions between the reactants (AB and H$_2$O) and catalyst (NiCu dimer) can be demonstrated by the energetically most favorable configurations shown in **Figure 2**. Although the AB hydrolysis reaction is complex in nature and it involves multistep mechanism, the configuration of the pre-equilibrium complex AB (reactants adsorbed on catalyst) is very important for the following reactions. By examining the possible adsorption styles of AB on NiCu dimer, including: –BH$_3$ (–NH$_3$) edge solely linked with Cu (Ni) atom; –BH$_3$ and –NH$_3$ edges synchronously linked with Cu and Ni atoms (and *vice versa*); B and N atoms directly linked with Cu (Ni) atom, we found that the configuration within –BH$_3$ edge approaching Ni atom is the most stable (R0). It is similar to the structure IM31 we proposed in previous literature (Zhou T. et al., 2016). The reason that –BH$_3$ edge prefers to bond with Ni atom instead of Cu atom can be understood from the Lewis base and acid reactions (Roach et al., 2009; Reber et al., 2010; Li et al., 2013). Since the overall negatively charged –BH$_3$ fragment [specifically for the hydridic H(B) donors] can be regarded as the Lewis base, it would like to interact with the positively charged Ni atom that can be regarded as the Lewis acid. In **Figure 2**, the highest occupied molecular orbital (HOMO), the lowest unoccupied molecular orbital (LUMO), and Mulliken atomic charges are presented on each structural configuration. From the point of view of the frontier orbital theory (Li and Evans, 1995), the LUMO/LUMO+1 site serves as the Lewis acid which will accept electrons readily, while the HOMO site serves as the Lewis base which will donate electrons. Consequently, –BH$_3$ edge would like to interact with Ni atom, because HOMO (LUMO) charge distribution is primarily localized around the –BH$_3$ fragment of AB molecule (Ni site of NiCu dimer).

FIGURE 1 | The reaction pathways of AB dehydrogenation without **(A)** and with **(C)** the catalyst Cu₂ dimer. The comparison of counterpart reactions in Gaussian and DMol³ software **(B,D)**.
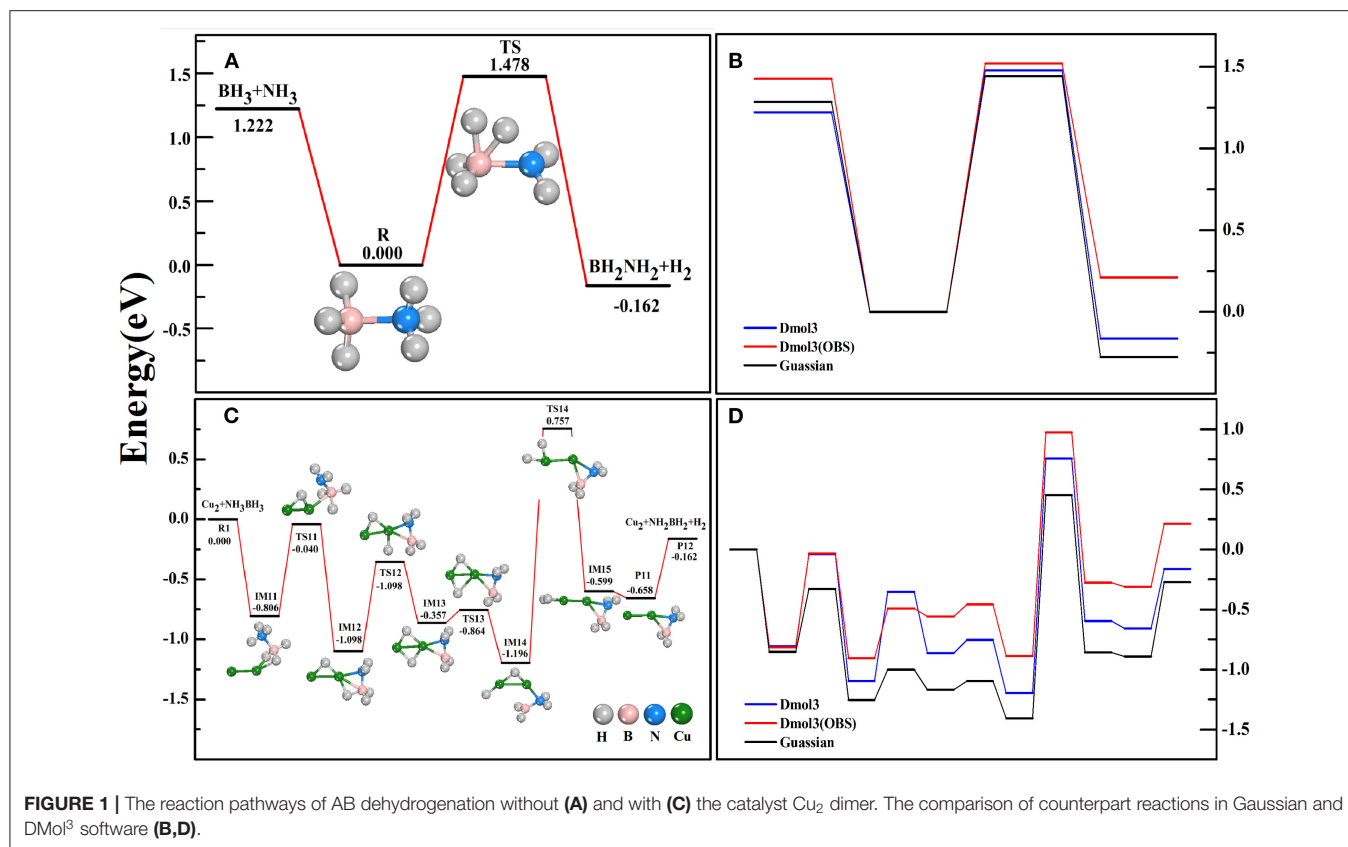
By inspecting the changes of bond-lengths between the adsorbed AB (R0) and the free AB, we found that two H-B bonds near Ni atom are elongated by 0.048 Å while one H-B bond far from Ni atom is compressed by 0.011 Å. The B-N bond is also compressed by 0.027 Å. There are the negligible changes for two of H-N bond-lengths on –NH₃ edge whereas the other H-N bond is stretched by 0.025Å. Since Ni/Cu atoms are positively/negatively charged in NiCu dimer, they would like to present the moderate interactions with different hydrogen species because the former/latter one is the hydridic-hydrogen/protic-hydrogen acceptor. After the adsorption, the hydridic H(B) atoms donate their partial electrons to Ni atom, resulting in H(B) atoms in the less negatively charged state (-0.178 e→-0.057 e). Meanwhile, the Ni atom back donates its electrons to B and Cu atoms, resulting in B atom in the less positively charged state (0.194 e→0.023 e) and Cu atom in the more negatively charged state (-0.038 e→-0.270 e). Note that the drawing force of Ni atom on its neighboring H(B) atoms has stretched the B-H bond-lengths. These activated H(B) atoms are then being ready for the subsequent dehydrogenation reactions owing to the formation of the agostic-bonds [B-H(B)···Ni] (Brookhart et al., 2007; Zins et al., 2015).

In the hydrolysis reaction process, it has been proposed that AB molecule firstly diffuses onto the catalyst surface and forms an activated intermediate. Upon the attack of a water molecule, the intermediate of AB molecule is dissociated to release H₂

(Chandra and Xu, 2006a,b; Xu and Chandra, 2006; Lu et al., 2013). Consequently, H₂O molecule should to adsorb on the AB-NiCu complex. Note that the adsorption of H₂O molecules plays a negligible role on the bond-lengths and bond-angles of AB fragment (R1 and R22 in **Figure 2**). For one H₂O adsorption in R1 configuration, one protic H(O) atom is bonded with both Ni and Cu atoms, stretching the corresponding H-O bond by 0.045 Å. If O atom is bonded with Ni atom, it is 0.183 eV higher in energy. For two H₂O adsorption in R22 configuration, O atom of the second H₂O with the lone-pair electrons will nucleophilically attack the well-defined electrophilic Ni site, because O atom tends to donate its lone-pair electrons to the LUMO and/or LUMO+1 orbitals around the Ni site (R1). Relative to O atom in free H₂O, we found that the O atom of the O-bonded H₂O in R22 losses 0.031 electrons (-0.489 e→-0.458 e) while the O atom of the H-bonded H₂O acquires 0.019 electrons (-0.489 e→-0.548 e). Although the R1 and R22 configurations present the negligible differences in bond-lengths and Mulliken charges, their HOMO (LUMO) charge distributions are significantly different. Previously, the investigation has proposed that the HOMO (LUMO) distributions can be used as a fine guidance to determine the sub-reaction pathway (Li et al., 2013). Here, the HOMO (LUMO) differences between R1 (one H₂O adsorption) and R22 (two H₂O adsorption) suggest that the stepwise and simultaneous H₂O attacking would give rise to different reaction pathways.

FIGURE 2 | The bond-length (in Å), Mulliken population charges (in e), as well as the schematic diagram of the frontier molecular orbitals (HOMO, LUMO/LUMO+1) for the energetically favorable reactant structures.
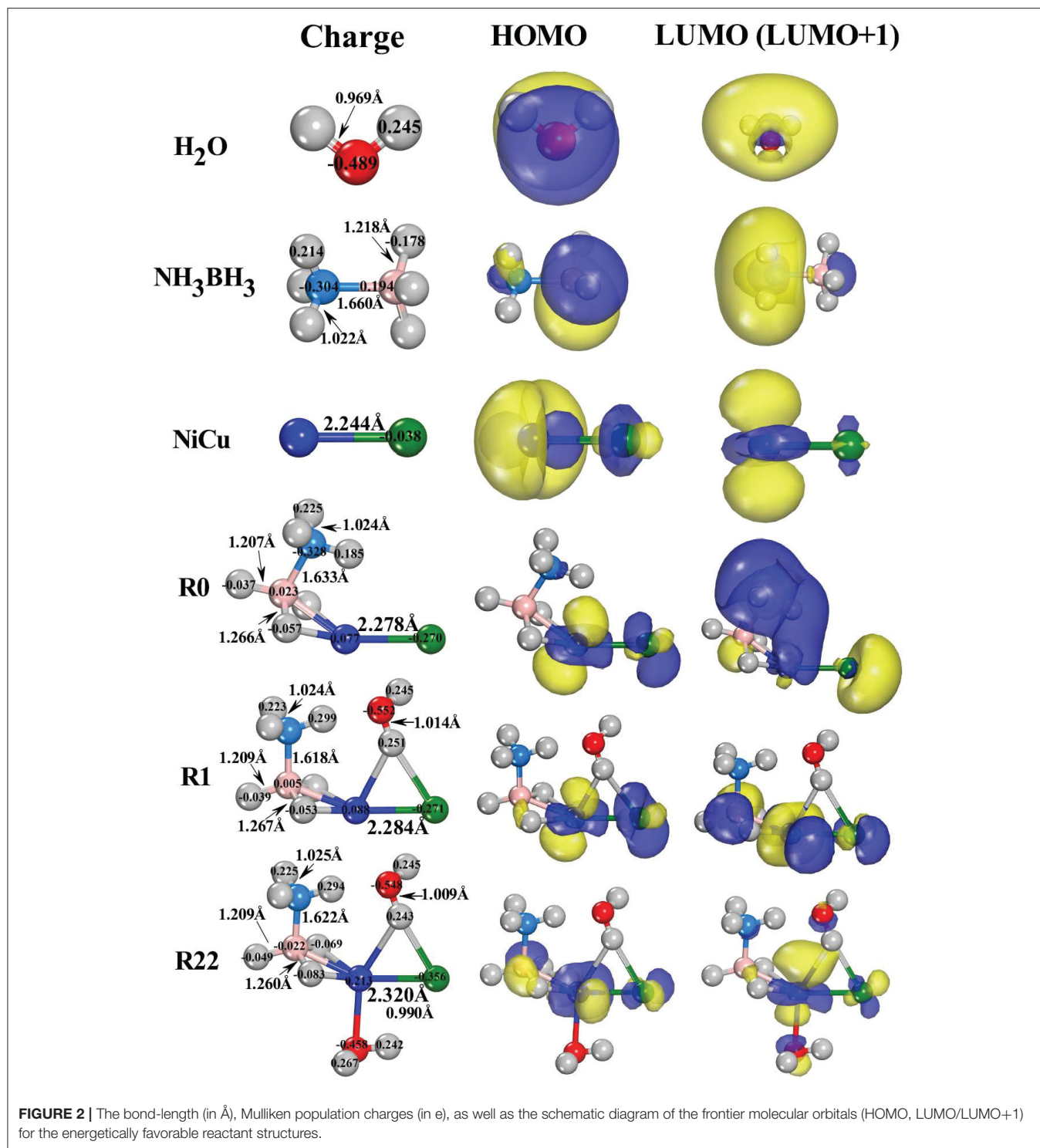
3.2. The Hydrolysis of AB Catalyzed by NiCu Dimer via the Stepwise H$_2$O Attack

In **Figures 3A–C**, we shown two preferential reaction pathways (path1 and path2) for the hydrolytic dehydrogenation of AB molecule catalyzed by NiCu dimer. These reactions undergo the stepwise attacks of H$_2$O molecules, named as H$_2$Ost, H$_2$Ond,

H$_2$Ord. The energies of R, IM, TS, P, together with their structural configurations were illustrated on each step. For the R1 reactant-complex that H$_2$Ost and AB molecules are simultaneously adsorbed on NiCu dimer (**Figure 3A**), it situates at an energy level of 1.587 eV below the initial reactants AB+H$_2$Ost+NiCu. In the next reaction step, the cationic Ni atom would like to
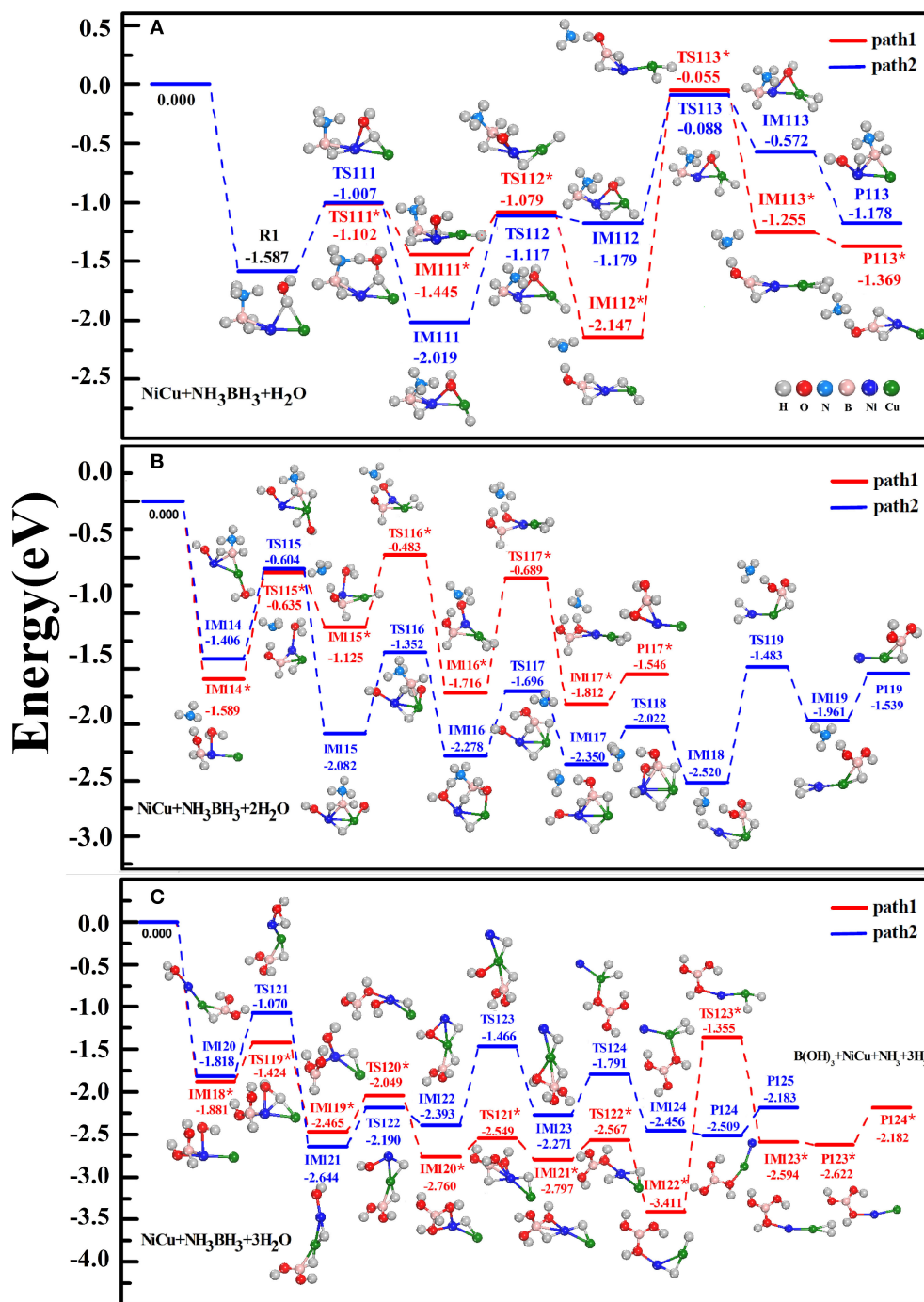
FIGURE 3 | Schematic energy profiles of hydrogen production from the catalytic hydrolysis of AB in the presence of NiCu dimer. The stepwise attacks involving three H$_2$O molecules, named as H$_2$Ost, H$_2$Ond, H$_2$Ord, are sequentially considered in **(A–C)**. The reactant, transition state, intermediate state, and product are denoted by R1, TS, IM, P, respectively.

interact with the nucleophilic [−OHst] but the anionic Cu atom would like to interact with the protic H(O) acceptor. Under the synergistical roles of Ni and Cu atoms, the H$_2$Ost molecule is decomposed into one hydrogen atom H(O) and one hydroxy group [−OHst] in IM111* or IM111 state. In terms of the reaction

principle for the bond activation, [−OHst] group will attack the positively charged B atom. If the O atom of [−OHst] hydroxy is close enough to the B atom, the stronger interactions between O and B atoms than between N and B atoms will split the B-N bond via the activation energy barrier of the TS112* state

(1.445–1.079 = 0.366 eV), i.e., –NH$_3$ is dissociated from BH$_3$-NH$_3$ fragment in IM112* state by releasing the energy of 2.147–1.079 = 1.068 eV. Previously, Banu et al. (2015) have found that when the H$_2$O molecule directly interacts with BH$_3$-NH$_3$ fragment yet without TM catalyst, the breaking of B-N bond at the assistant of [-OH] group needs to cross a very high energy barrier of 1.19 eV, and the counterpart TS state is even 0.91 eV above the separated reactants AB+H$_2$O. Clearly, the present of NiCu dimer can significantly reduce the activation energy barrier during the hydrolytic AB. If the O-B interaction doesn't play the role this time, the O atom maintains its interactions with Ni and Cu atom in IM112 state (presenting a three-membered Ni-O-Cu ring). Whichever the reaction it happens, one H(B) atom of AB is somewhat activated by Ni atom and being ready to adsorb on Cu atom, because the corresponding H-B bond in IM112* is elongated by 0.169 Å (elongated by 0.056Å in IM112) with respect to 1.218 Å of free AB. Following the IM112* or IM112 state, H(O) and H(B) atoms on Cu atom move close to each other to form a Cu-dihydride complex in IM113* state or IM113 state. Ultimately, the H$_2^{(st)}$ molecule is released from the first-step-product P113* ([OH]·BH$_2$·NiCu+NH$_3$+H$_2$) or product P113 ([OH]·NiCu·NH$_3$BH$_2$+H$_2$), which releases the energy of 0.114 or 0.606 eV.

Apart from the above dehydrogenation pathways, we have considered other reaction routes from the R1 reactants: the first dissociation of H(B) atom and then H(O) atom; the stepwise dissociations of H(N) and H(O) atoms. However, these reaction routes have not any superiority with respect to the path1 and path2. For example, the reaction that one H(B) atom in R1 is activated and interacted with Cu atom has to go across a very high energy barrier (1.146 eV). It is 0.789 eV higher in energy than IM111* state. There are the possibilities that the released H$_2$ molecule is comprised of H(B) and H(N) atoms from AB fragment, which is analogous to what we have proposed in Zhou T. et al. (2016). Nevertheless, our primary goal is to explore the reaction mechanism that the hydrolytic dehydrogenation is happening with the assistant of H$_2$O. Consequently, these routes have been discarded owing to no dissociation of H(O) atom from H$_2$O. As a mater of fact, Shevlin et al. (2011) have indicated that the dehydrogenation via the combination of the protic atoms from the N-moiety and the hydridic atoms from the B-moiety is energetically unfavored for the metal amidoboranes MNH$_2$BH$_3$. In addition, another possible pathway could follow the IM111* or IM111 states: (i) One H(N) atom transfers to [–OH] group to produce the adsorbed H$_2$O and BH$_3$-NH$_2$ fragment once again; (ii) One H(O) atom is dissociated from the H$_2$O and then shifted to Cu atom, forming the Cu-dihydride complex and [–OH] group; (iii) The B-N bond of BH$_3$-NH$_2$ fragment is broken by [–OH] group, yielding the NH$_2$ and H$_2$ products. However, the B-N bond has an obvious contraction as one H(N) atom was migrated from –NH$_3$ edge after the first step reaction. It will be of ever-increasing difficulty to break the B-N bond by [–OH] group. Typically and importantly, the released product of NH$_2$ in this pathway does not agree with the experimental product of NH$_3$ (Yao C. F. et al., 2008; Rachiero et al., 2011b; Chou et al., 2012; Liu et al., 2012).

For the adsorption of the second H$_2$Ond on the first-step-products, both Ni and Cu atoms are considered as the tentatively adsorbing sites. Our calculations demonstrate that the Ni site is 0.176 eV lower in energy than the Cu site in adsorbing O atom for the product P113*, whereas it reverses for the product P113. In **Figure 3B**, we show the subsequent reactions that the first-step-products are attacked by the H$_2$Ond. The crucial reaction steps for the path1 are follows: (i) One of two hydridic H(B) atoms in IM114* is activated by the Lewis acid of Ni atom, and then it is optimally adsorbed on Cu atom in the formation of Cu-monohydride complex in IM115*; (ii) The protic H(O) atom and [-OHnd] of the H$_2$Ond are synergistically activated by Cu and Ni atoms, and then this protic H(O) atom shifts to Cu atom yielding the Cu-dihydride complex in IM116*; (iii) The [-OHnd] group moves close to B atom to form the B-dihydroxy and Cu-dihydride fragments in IM117*, which is followed by the releasing of H$_2^{(nd)}$ molecule (the second-step-products P117*). For the successive reactions along the path2, there presents a thermodynamically downhill trend from IM114 to IM118 as well as from TS115 to TS118, revealing that these reactions would take place spontaneously due to their overall exothermic processes. In analogous with the dehydrogenation mechanism involving the H$_2$Ost attack, three critical processes can be clearly concerned for the H$_2$Ond attack: (i) The protic H(O) atom is somewhat activated by Ni atom and then it links with both Ni and Cu atoms in IM115; (ii) The [-OHnd] group breaks the N-B bond and dissociate –NH$_3$ fragment through IM116 to IM117; (iii) The B-dihydroxy and Ni-dihydride complex comes into being through IM118 to IM119, from which H$_2^{(nd)}$ is subsequently liberated (second-step-products P119). Generally speaking, since each energy barrier can be crossed at the available energies provided by the exothermic reaction, the overall reactions are thermodynamically feasible for either path1 or path2. Nevertheless, P119 state is the predomination state, because each IM state together with the counterpart TS state in path2 lies lower in energy than that in path1.

After the adsorption of the third H$_2$Ord on the second-step-products (**Figure 3C**), IM118* and IM120 states come into being, respectively. Again, Ni atom serves as the activation site for dissociating H(O) atom from H$_2$Ord, and its neighboring Cu atom serves as the attractive site for adsorbing H(O) atom. The last H(B) atom is gradually transferred to Cu atom to form the Cu-dihydride fragment. It is synchronously/succesively accompanied by the shifting of [-OHrd] group from Ni atom to B atom (forming the B-trihydroxy fragment) and by the releasing of H$_2^{(rd)}$ molecule. All IM and TS states are accessible for proceeding the dehydrogenation reactions. Viewing the pathway as a whole, we found that TS113* and TS113 states are only 0.055 and 0.088 eV lower in energy than the initial reactants. Since they present the highest energy barriers, these states are the rate determining barriers of the overall dehydrogenation processes. Nevertheless, it is nothing to be worried about this requirement, because the foregoing reactions are overall exothermic process and TS113* and TS113 states can be overcome. Ultimately, the hydrolytic dehydrogenation reaction is completed, NH$_3$BH$_3$+3H$_2$O $\xrightarrow{\text{NiCu}}$

FIGURE 4 | Schematic energy profiles of catalytic hydrolysis of AB involving the simultaneous H_2O attacks **(A)**. The hydrolysis AB is simultaneously attacked by $H_2O^{(1)}$ and $H_2O^{(2)}$ **(B)** and subsequently attacked by $H_2O^{(3)}$ **(C)**.
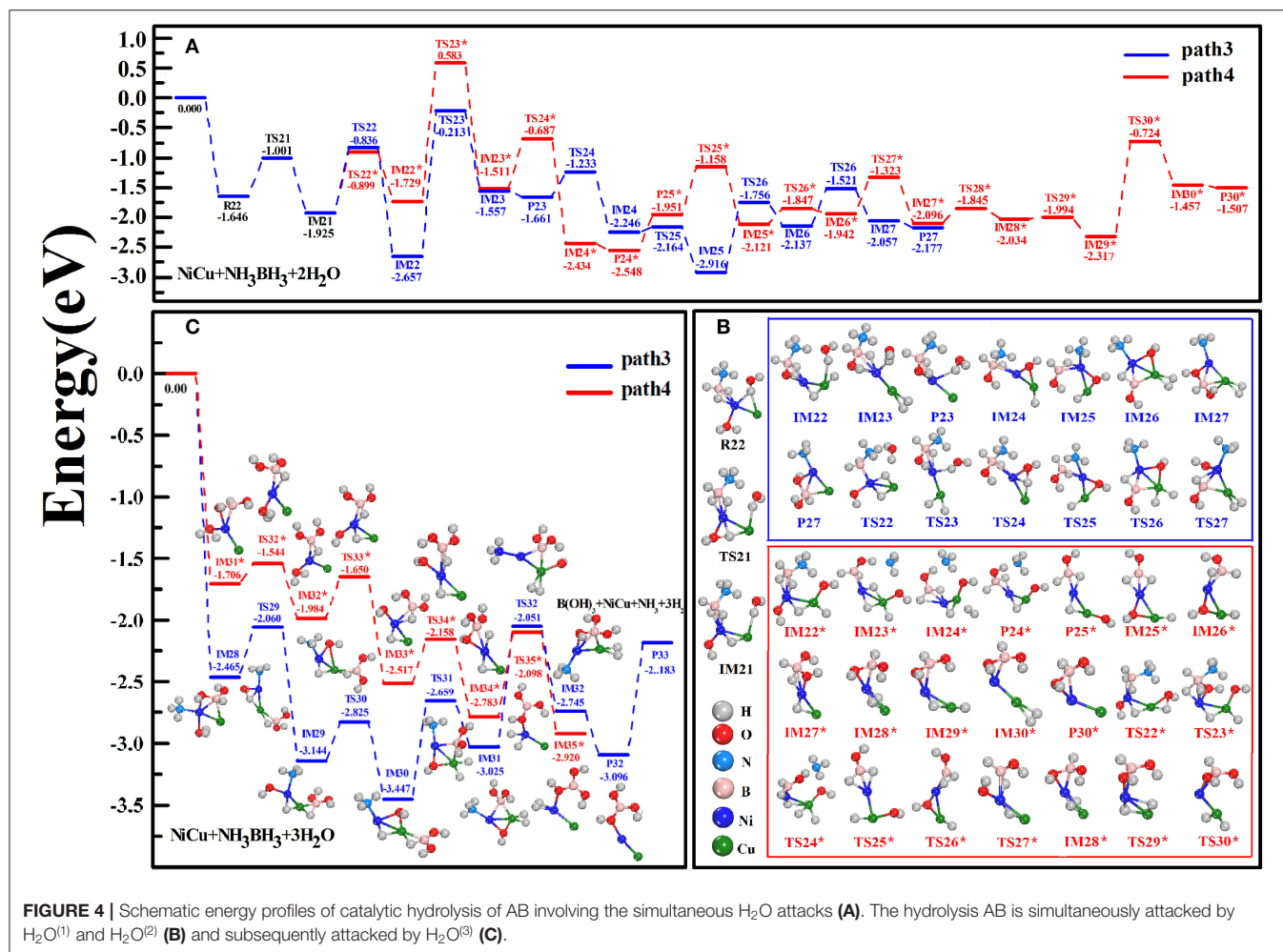
NiCu·NH₃+B(OH)₃+3H₂↑, which is catalyzed by the NiCu dimer and orderly attacked by three H_2O molecules. We can conclude that *the formation of Cu-dihydride and B-multihydroxy fragments in IM states is crucial for the hydrolytic dehydrogenation, and both metal atoms are acted as the catalytic sites for breaking the H-O bond of H_2O and N-B bond of NH_3BH_3.*

3.3. The Hydrolysis of AB Catalyzed by NiCu Dimer via the Simultaneous H_2O Attack

For the hydrolytic AB via the simultaneous adsorption of a few H_2O molecules, we considered the reaction case: AB is simultaneously attacked by $H_2O^{(1)}$ and $H_2O^{(2)}$ and subsequently attacked by $H_2O^{(3)}$. In the configuration of R22 reactant (**Figure 4B**), $H_2O^{(1)}$ with O atom is attached to Ni atom while $H_2O^{(2)}$ with H atom is bridged with Cu and Ni atoms. From R22 to IM22 states along the path3, one H-O bond of $H_2O^{(1)}$ and one H-B bond of AB are successively broken. Then, H(O) and H(B) atoms are bonded with Cu atom to generate the Cu-dihydride complex

and [–OH]$^{(1)}$ group, following which the B-monohydroxy complex (IM22) comes into being. In this situation, N-B bond-length is elongated by 0.050 Å with respect to 1.622 Å in R22. For the subsequent reaction from IM22 to IM23, $H_2O^{(2)}$ is shifted from Cu site to Ni site. After releasing the first $H_2^{(st)}$ in P23, several steps related to the atomic transfers are crucial: (i) One H(O) atom of $H_2O^{(2)}$ is dissociated and subsequently bonded with Cu atom (IM24), yielding [–OH]$^{(2)}$ group that is ready to break the N-B bond of AB (IM25); (ii) One H(B) atom gradually moves to Cu atom to generate the Cu-dihydride (IM26), which is the prerequisite in releasing the second $H_2^{(nd)}$ (P27); (iii) The adsorption site of [–OH]$^{(2)}$ is adjusted to connect with B atom (TS27), which contributes to the B-dihydroxy fragments (IM27). Thus, above reactions can be described as: $NH_3BH_3+2H_2O \xrightarrow{NiCu} NiCu·NH_3···HB(OH)_2+2H_2\uparrow$. When $H_2O^{(3)}$ is adsorbed on the resulting product P27 (**Figure 4C**), analogously, one H(O) atom of $H_2O^{(3)}$ and the last H(B) atom are gradually transferred to Cu atom (from IM29 to IM31). It is followed by the movement of [–OH]$^{(3)}$ group to B site, again yielding the Cu-dihydride and B-trihydroxy

complex (IM32). Then, the releases of NH_3 and $H_2^{(rd)}$ via P32 and P33 states can be achieved. Finally, we complete the experimental reactions in an overall exothermic and barrierless pathway, $NH_3BH_3+3H_2O \xrightarrow{NiCu} NH_3+NiCu \cdot B(OH)_3+3H_2 \uparrow$. On the whole, the key mechanism of the path3 is that H(O) and H(B) atoms are alternately

dissociated from H_2O and AB molecules, successively yielding Cu-dihydride and B-multihydroxy complexes in IM states.

Unlike the dehydrogenation mechanism of the path3, we consider the reaction path 4 that two H(O) atoms are firstly detached from $H_2O^{(1)}$ and $H_2O^{(2)}$ (IM22*) and then H(B)
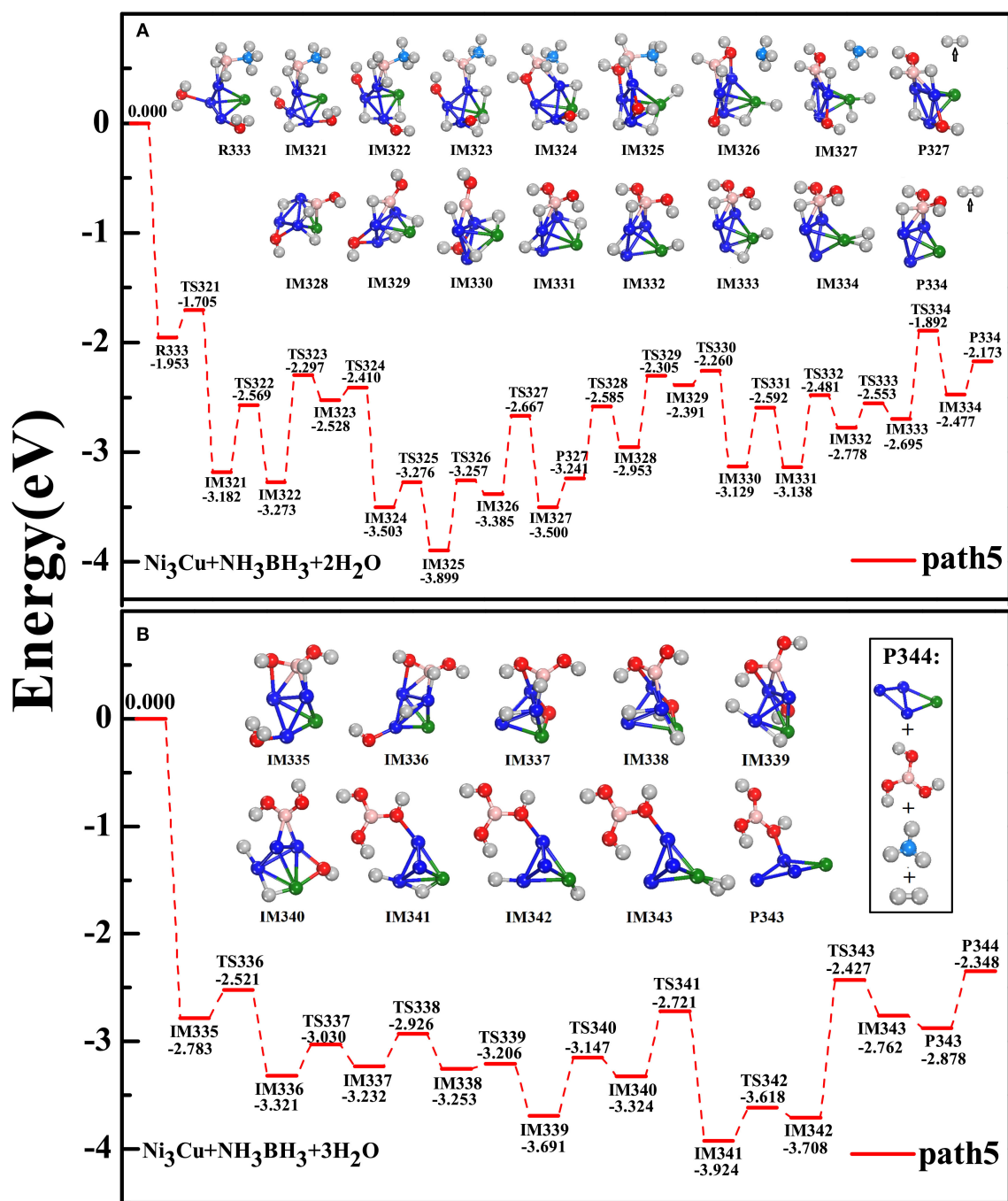
FIGURE 5 | Similar to that of **Figure 4** but for the catalyst of Ni₃Cu tetramer: **(A)** hydrolysis of AB simultaneously attacked by $H_2O^{(1)}$ and $H_2O^{(2)}$; **(B)** subsequently attacked by the third $H_2O^{(3)}$.

atoms are departed from AB molecule (IM24*). However, high energy barrier of 1.729–0.583 = 1.146 eV is encountered at TS23* state when [−OH][(1)] group acts as an attacker to dissociate −NH$_3$ fragment (IM23*). Although this reaction step is thermodynamically unfeasible, to verify our findings that the hydrolytic dehydrogenation reaction undergoes via the specific intermediate states, we continue the reactions irrespective of TS23* state. To one's expectation, the formations of the Cu-dihydride complexes (IM24*, IM30*, and IM35*) together with the B-multihydroxy complexes (IM23*, IM27*, IM34*) can be clearly discerned from the sequential steps in **Figures 4B,C**. Experimentally, the activation energy for the catalytic hydrolysis of AB dehydrogenation has been conjectured to be the step reaction of B-N bond breaking (Xu and Chandra, 2006; Chandra and Xu, 2007), where an apparent value was estimated around 0.4 eV for CuNi catalysts (Lu et al., 2014; Zhang et al., 2016). Our E$_{act}$ = 0.58 eV determined by the highest energy barrier of the reaction path4 at TS113* state is approach to these experimental activation energies. Here, we found that the hydride transfer is responsible for the rate-determining step for all pathways we studied.

3.4. The Hydrolysis of AB Catalyzed by Ni$_3$Cu Cluster via the Simultaneous H$_2$O Attack

Since the tetrahedral structure is the block-unit for constructing large metal nanoclusters, Ni$_3$Cu tetrahedron cluster is treated as an ideal model to underline the catalysis effect on the hydrolytic dehydrogenation of AB. Importantly, experimental synthesizing has shown the Cu@Ni core-shell structure, where Ni atoms are on the structural surface and as the active sites (Lu et al., 2014; Zhang et al., 2016). After considering the different adsorption styles, i.e., -BH$_3$ fragment (or -NH$_3$ fragment) is adjacent to Ni atom (or Cu atom) as well as H$_2$O[(1)] and H$_2$O[(2)] molecules are attached on various metal sites, we found that R333 configuration is the most favorable adsorption style (**Figure 5**). Although the reaction steps are more and complex in the present of Ni$_3$Cu cluster, according to the criterion of the dehydrogenation that the reactions should follow the pathway in an exothermic, overall barrierless, and the minimum energy profile, we found that the accessible pathway for the catalytic dehydrogenation by Ni$_3$Cu cluster is exactly identical to that by NiCu dimer. The subsequent reaction steps are following: the alternation of the breaking of three H-O bonds from three H$_2$O molecules (IM321, IM322, IM336) with the breaking of three B-H bonds from AB molecule (IM323, IM328, IM338); the dissociation of NH$_3$ from AB molecule (IM326); the adjustment of the adsorbing sites of H(O) and H(B) atoms and [-OH] groups to yield the metal-dihydride and B-multioxhydryl fragment (IM327, IM334, IM343); the liberation of three H$_2$ molecules through three intermediate products (P327, P334, P343); the recovery of Ni$_3$Cu catalyst after the complete reactions (P344). Throughout all procedures of the path5, the hydrolytic dehydrogenation process is feasible both in kinetics and thermodynamics: NH$_3$BH$_3$+3H$_2$O $\xrightarrow{\text{Ni}_3\text{Cu}}$ Ni$_3$Cu·NH$_3$BH$_3$···(H$_2$O)$_3$ → Ni$_3$Cu·NH$_3$+B(OH)$_3$+3H$_2$↑.

FIGURE 6 | The proposed schematic representation of hydrolytic AB for hydrogen generation in the presence of metal catalyst: **(A)** hydrolysis of AB catalyzed by metal catalyst via the stepwise H$_2$O attack; **(B)** hydrolysis of AB by metal catalyst via the simultaneous H$_2$O attack.
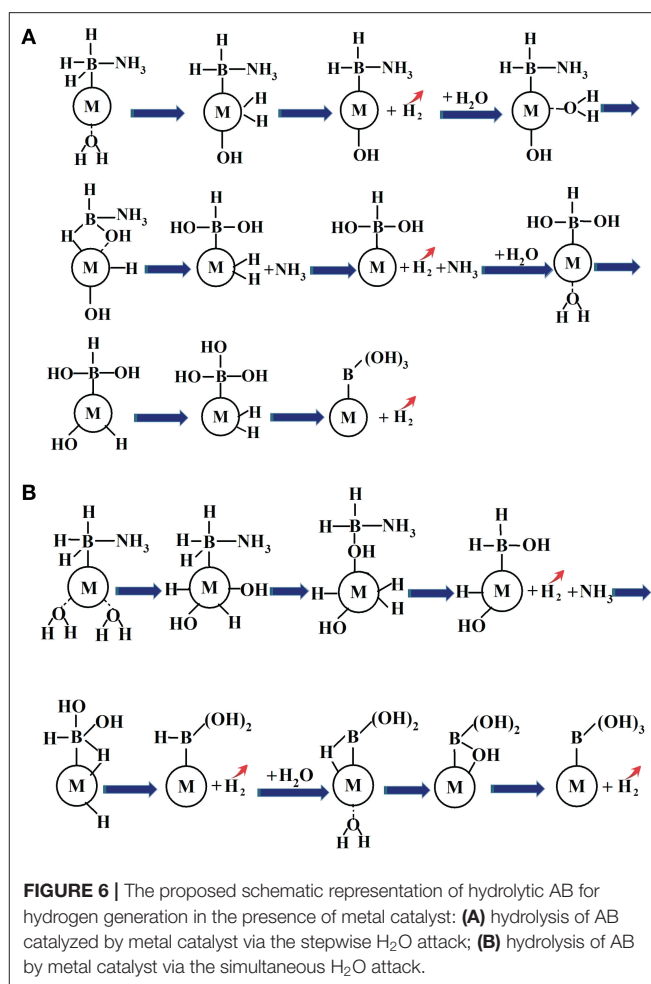
4. CONCLUSIONS

A novel reaction strategy to the prediction of the dehydrogenation sequences for catalytic hydrolysis of AB by NiCu bimetal catalyst has been developed, NH$_3$BH$_3$+3H$_2$O $\xrightarrow{\text{NiCu}}$ NiCu·NH$_3$+B(OH)$_3$+3H$_2$↑, and the plausible mechanisms were analyzed under a molecular level by using the density functional theory method. Our proposed catalytic hydrolysis of AB for the hydrogen generation are illustrated in **Figure 6**.

The driving force behind the formations of NH$_3$ and H$_2$ is the development of [-OH] group and Cu-dihydride complex species after the H$_2$O participation. The former resultant attack the B-N bond to dissociate NH$_3$ and the latter resultant is the prerequisite toward the H$_2$ elimination. The activation energy barrier for the hydrolytic AB is most likely caused by the hydride transfer from H(B) to metal atom rather than the B-N bond breaking. The formation of heterometallic NiCu bonds and the charge transfers might be the key factor to tune the frontier molecular orbitals of the catalyst surface atom, which play the decisive role to react with the molecules (AB and H$_2$O) and to stabilize the possible intermediate states, leading to the improved catalytic activity

and selectivity in comparison with those of the corresponding monometallic counterparts.

DATA AVAILABILITY STATEMENT

All datasets generated for this study are included in the article/supplementary material.

AUTHOR CONTRIBUTIONS

WY, YZ, and TZ: software and writing-original draft preparation. GW: software, writing-original draft preparation, and methodology. DW: writing-reviewing and editing. HY: software, writing-original draft preparation, methodology, writing-reviewing and editing, and conceptualization. All authors contributed to the article and approved the submitted version.

FUNDING

REFERENCES

Ayala, P. Y., and Schlegel, H. B. (1997). A combined method for determining reaction paths, minima, and transition state geometries. *J. Chem. Phys.* 107, 375–384. doi: 10.1063/1.474398

Banu, T., Debnath, T., Ash, T., and Das, A. K. (2015). Hydrolysis of ammonia borane and metal amidoboranes: a comparative study. *J. Chem. Phys.* 143, 194305–194305. doi: 10.1063/1.4935933

Basu, S., Zheng, Y., Varma, A., Delgass, W. N., and Gore, J. P. (2010). Catalytic hydrolysis of ammonia borane: intrinsic parameter estimation and validation. *J. Power Sources* 195, 1957–1963. doi: 10.1016/j.jpowsour.2009.10.070

Becke, A. D. (1988). Density-functional exchange-energy approximation with correct asymptotic behavior. *Phys. Rev. A* 38, 3098–3100. doi: 10.1103/PhysRevA.38.3098

Brockman, A., Zheng, Y., and Gore, J. (2010). A study of catalytic hydrolysi s of concentrated ammonia borane solution. *Int. J. Hydrogen Energy* 35, 7350–7356. doi: 10.1016/j.ijhydene.2010.04.172

Brookhart, M., Green, M. L. H., and Parkin, G. (2007). Agostic interactions in transition metal compounds. *Proc. Natl. Acad. Sci. U.S.A.* 104, 6908–6914. doi: 10.1073/pnas.0610747104

Bučko, T., Hafner, J., Lebègue, S., and Angyan, J. G. (2010). Improved description of the structure of molecular and layered crystals: ab initio DFT calculations with van der Waals corrections. *J. Phys. Chem. A* 114, 11814–11824. doi: 10.1021/jp106469x

Can, H., and Metin, Ö. (2012). A facile synthesis of nearly monodisperse ruthenium nanoparticles and their catalysis in the hydrolytic dehydrogenation of ammonia borane for chemical hydrogen storage. *Appl. Catal. B Environ.* 125, 304–310. doi: 10.1016/j.apcatb.2012.05.048

Chandra, M., and Xu, Q. (2006a). A high-performance hydrogen generation system: transition metal-catalyzed dissociation and hydrolysis of ammonia-borane. *J. Power Sources* 156, 190–194. doi: 10.1016/j.jpowsour.2005.05.043

Chandra, M., and Xu, Q. (2006b). Dissociation and hydrolysis of ammoniaeborane with solid acids and carbon dioxide: an efficient hydrogen generation system. *J. Power Sources* 159, 855–860. doi: 10.1016/j.jpowsour.2005.12.033

Chandra, M., and Xu, Q. (2007). Room temperature hydrogen generation from aqueous ammonia-borane using noble metal nanoclusters as highly active catalysts. *J. Power Sources* 168, 135–142. doi: 10.1016/j.jpowsour.2007.03.015

Chen, F., Ma, H., Li, Y., and Chen, J. (2007). Ni$_{1-x}$Pt$_x$ ($x = 0$–0.12) hollow spheres as catalysts for hydrogen generation from ammonia borane. *Inorg. Chem.* 46, 788–794. doi: 10.1021/ic061712e

Chen, G., Desinan, S., Nechache, R., Rosei, R., Rosei, F., and Ma, D. (2011). Bifunctional catalytic/magnetic Ni@Ru core-shell nanoparticles. *Chem. Commun.* 47, 6308–6310. doi: 10.1039/c1cc10619h

Chen, G., Desinan, S., Rosei, R., Rosei, F., and Ma, D. (2012). Synthesis of Ni-Ru alloy nanoparticles and their high catalytic activity in dehydrogenation of ammonia borane. *Chem. Eur. J.* 18, 7925–7930. doi: 10.1002/chem.201200292

Chen, W., Ji, J., Feng, X., Duan, X., Qian, G., Li, P., et al. (2014). Mechanistic insight into size-dependent activity and durability in Pt/CNT catalyzed hydrolytic dehydrogenation of ammonia borane. *J. Am. Chem. Soc.* 136, 16736–16739. doi: 10.1021/ja509778y

Chou, C., Lee, D., and Chen, B. (2012). Hydrogen production from hydrolysis of ammonia borane with limited water supply. *Int. J. Hydrogen Energy* 37, 15681–15690. doi: 10.1016/j.ijhydene.2012.05.108

Chua, Y. S., Chen, P., Wu, G., and Xiong, Z. (2011). Development of amidoboranes for hydrogen storage. *Chem. Commun.* 47, 5116–5129. doi: 10.1039/C0CC05511E

Çiftci, N. S., and Metin, Ö. (2014). Monodisperse nickel-palladium alloy nanoparticles supported on reduced graphene oxide as highly efficient catalysts for the hydrolytic dehydrogenation of ammonia borane. *Int. J. Hydrogen Energy* 39, 18863–18870. doi: 10.1016/j.ijhydene.2014.09.060

Delley, B. (2000). From molecules to solids with the DMol³ approach. *J. Chem. Phys.* 113, 7756–7764. doi: 10.1063/1.1316015

Demirci, U. B., and Miele, P. (2009). Sodium borohydride versus ammonia borane, in hydrogen storage and direct fuel cell applications. *Energy Environ. Sci.* 2, 627–637. doi: 10.1039/B900595A

Demirci, U. B., and Miele, P. (2010). Hydrolysis of solid ammonia borane. *J. Power Sources* 195, 4030–4035. doi: 10.1016/j.jpowsour.2010.01.002

Dinç, M., Metin, Ö., and Özkar, S. (2012). Water soluble polymer stabilized iron(0) nanoclusters: a cost-effective and magnetically recoverable catalyst in hydrogen generation from the hydrolysis of sodium borohydride and ammonia borane. *Catal. Today* 183, 10–16. doi: 10.1016/j.cattod.2011.05.007

Güngörmez, K., and Metin, Ö. (2015). Composition-controlled catalysis of reduced graphene oxide supported CuPd alloy nanoparticles in the hydrolytic dehydrogenation of ammonia borane. *Appl. Catal. A* 494, 22–28. doi: 10.1016/j.apcata.2015.01.020

Hamilton, C. W., Baker, R. T., Staubitz, A., and Manners, I. (2009). B-N compounds for chemical hydrogen storage. *Chem. Soc. Rev.* 38, 279–293. doi: 10.1039/b800312m

Hirshfeld, F. L. (1977). Bonded-atom fragments for describing molecular charge densities. *Theor. Chem. ACC.* 44, 129–138. doi: 10.1007/BF00549096

Hu, M. G., Geanangel, R. A., and Wendlandt, W. W. (1978). The thermal decomposition of ammonia borane. *Thermochim Acta* 23, 249–255. doi: 10.1016/0040-6031(78)85066-7

Huang, Z., and Autrey, T. (2012). Boron-nitrogen-hydrogen (BNH) compounds: recent developments in hydrogen storage, applications in hydrogenation and catalysis, and new syntheses. *Energy Environ. Sci.* 5, 9257–9268. doi: 10.1039/c2ee23039a

Jiang, H., and Xu, Q. (2011). Catalytic hydrolysis of ammonia borane for chemical hydrogen storage. *Catal. Today* 170, 56–63. doi: 10.1016/j.cattod.2010.09.019

Jiang, H. L., Umegaki, T., Akita, T., Zhang, X. B., Haruta, M., and Xu, Q. (2010). Bimetallic Au-Ni nanoparticles embedded in SiO₂ nanospheres: synergetic catalysis in hydrolytic dehydrogenation of ammonia borane. *Chem. Eur. J.* 16, 3132–3137. doi: 10.1002/chem.200902829

Kalidindi, S. B., Indirani, M., and Jagirdar, B. R. (2008a). First row transition metal ion-assisted ammoniaeborane hydrolysis for hydrogen generation. *Inorg. Chem.* 47, 7424–7429. doi: 10.1021/ic800805r

Kalidindi, S. B., Sanyal, U., and Jagirdar, B. R. (2008b). Nanostructured Cu and Cu@Cu₂O core shell catalysts for hydrogen generation from ammonia-borane. *Phys. Chem. Chem. Phys.* 10, 5870–5874. doi: 10.1039/B805726E

Karahan, S., Zahmakiran, M., and Özkar, S. (2012). A facile one-step synthesis of polymer supported rhodium nanoparticles in organic medium and their catalytic performance in the dehydrogenation of ammonia-borane. *Chem. Commun.* 48, 1180–1182. doi: 10.1039/C1CC15864C

Kılıç, B., Şencanlı, S., and Metin, Ö. (2012). Hydrolytic dehydrogenation of ammonia borane catalyzed by reduced graphene oxide supported monodisperse palladium nanoparticles: high activity and detailed reaction kinetics. *J. Mol. Catal. A-Chem.* 361, 104–110. doi: 10.1016/j.molcata.2012.05.008

Komova, O. V., Kayl, N. L., Odegova, G. V., Netskina, O. V., and Simagina, V. I. (2016). Destabilization of NH_3BH_3 by water during hydrothermolysis as a key factor in the high hydrogen evolution rates. *Int. J. Hydrogen Energy* 41, 17484–17495. doi: 10.1016/j.ijhydene.2016.07.163

Li, F., Sun, L. X., Zhao, J. J., Xu, F., Zhou, H. Y., Zhang, Q. M., et al. (2013). Mechanisms of H_2 generation for metal doped Al_{16} M (M = Mg and Bi) clusters in water. *Int. J. Hydrogen Energy* 38, 6930–6937. doi: 10.1016/j.ijhydene.2013.03.076

Li, Y., and Evans, J. N. S. (1995). The fukui function: a key concept linking frontier molecular orbital theory and the hard-soft-acid-base principle. *J. Am. Chem. Soc.* 117, 7756–7759. doi: 10.1021/ja00134a021

Li, Z., He, T., Liu, L., Chen, W. D., Zhang, M., Wu, G.T., et al. (2017). Covalent triazine framework supported non-noble metal nanoparticles with superior activity for catalytic hydrolysis of ammonia borane: from mechanistic study to catalyst design. *Chem. Sci.* 8, 781–788. doi: 10.1039/C6SC02456D

Liang, H. Y., Chen, G. Z., Desinan, S., Rosei, R., Rosei, F., and Ma, D. L. (2012). In situ facile synthesis of ruthenium nanocluster catalyst supported on carbon black for hydrogen generation from the hydrolysis of ammoniaeborane. *Int. J. Hydrogen Energy* 37, 17921–17927. doi: 10.1016/j.ijhydene.2012.09.026

Liu, C., Wu, Y., Chou, C., Chen, B., Hsueh, C., Ku, J., et al. (2012). Hydrogen generated from hydrolysis of ammonia borane using cobalt and ruthenium based catalysts. *Int. J. Hydrogen Energy* 37, 2950–2959. doi: 10.1016/j.ijhydene.2011.05.022

Lu, Z. H., Jiang, H. L., Yadav, M., Aranishi, K., and Xu, Q. (2012). Synergistic catalysis of Au-Co@SiO2 nanospheres in hydrolytic dehydrogenation of ammonia borane for chemical hydrogen storage. *J. Mater. Chem.* 22, 5065–5071. doi: 10.1039/c2jm14787d

Lu, Z. H., Li, J., Feng, G., Yao, Q., Zhang, F., Zhou, R., et al. (2014). Synergistic catalysis of MCM-41 immobilized Cu-Ni nanoparticles in hydrolytic dehydrogeneration of ammonia borane. *Int. J. Hydrogen Energy* 39, 13389–13395. doi: 10.1016/j.ijhydene.2014.04.086

Lu, Z. H., Li, J., Zhu, A., Yao, Q., Huang, W., Zhou,R., et al. (2013). Catalytic hydrolysis of ammonia borane via magnetically recyclable copper iron nanoparticles for chemical hydrogen storage. *Int. J. Hydrogen Energy* 38, 5330–5337. doi: 10.1016/j.ijhydene.2013.02.076

Lu, Z. H., and Xu, Q. (2012). Recent progress in boron- and nitrogen-based chemical hydrogen storage. *Funct. Mater. Lett.* 5, 1230001–1230009. doi: 10.1142/S1793604712300010

Matus, M. H., Anderson, K. D., Camaioni, D. M., Autrey, S. T., and Dixon, D. A. (2007). Reliable predictions of the thermochemistry of boron-nitrogen hydrogen storage compounds: $B_xN_xH_y$, $x = 2$, 3. *J. Phys. Chem. A* 111, 4411–4421. doi: 10.1021/jp070931y

Metin, O., Duman, S., Dinc, M., and Ozkar, S. (2011). Oleylamine-stabilized palladium(0) nanoclusters as highly active heterogeneous catalyst for the dehydrogenation of ammonia borane. *J. Phys. Chem. C* 115, 10736–10743. doi: 10.1021/jp201906n

Metin, Ö., Mazumder, V., Özkar, S., and Sun, S. (2010). Monodisperse nickel nanoparticles and their catalysis in hydrolytic dehydrogenation of ammonia borane. *J. Am. Chem. Soc.* 132, 1468–1469. doi: 10.1021/ja909243z

Metin, Ö., and Özkar, S. (2011). Water soluble nickel(0) and cobalt(0) nanoclusters stabilized by poly(4-styrenesulfonic acid-comaleic acid): highly active, durable and cost effective catalysts in hydrogen generation from the hydrolysis of ammonia borane. *Int. J. Hydrogen Energy* 36, 1424–1432. doi: 10.1016/j.ijhydene.2010.10.070

Mohajeri, N., Ali, T., and Adebiyi, O. (2007). Hydrolytic cleavage of ammonia-borane complex for hydrogen production. *J. Power Sources* 167, 482–485. doi: 10.1016/j.jpowsour.2007.02.059

Patel, N., and Miotello, A. (2015). Progress in Co-B related catalyst for hydrogen production by hydrolysis of boron-hydrides: a review and the perspectives to substitute noble metals. *Int. J. Hydrogen Energy* 40, 1429–1464. doi: 10.1016/j.ijhydene.2014.11.052

Peng, B., and Chen, J. (2008). Ammonia borane as an efficient and lightweight hydrogen storage medium. *Energy Environ. Sci.* 1, 479–483. doi: 10.1039/B809243P

Peng, C., Ayala, P. Y., Schlegel, H. B., and Frisch, M. J. (1996). Using redundant internal coordinates to optimize equilibrium geometries and transition states. *J. Comput. Chem.* 17, 49–56. doi: 10.1002/(sici)1096-987x(19960115)17:1<49::aid-jcc5>3.0.co;2-0

Peng, C., and Schlegel, H. B. (1993). Combining Synchronous Transit and Quasi-Newton Methods to Find Transition States. *Isr. J. Chem.* 33, 449–454. doi: 10.1002/ijch.199300051

Perdew, J. P., and Wang, Y. (1992). Accurate and simple analytic representation of the electron-gas correlation energy. *Phys. Rev. B* 45, 13244–132499. doi: 10.1103/PhysRevB.45.13244

Rachiero, G. P., Demirci, U. B., and Miele, P. (2011a). Facile synthesis by polyol method of a ruthenium catalyst supported on γ-Al_2O_3 for hydrolytic dehydrogenation of ammonia borane. *Catal. Today* 170, 85–92. doi: 10.1016/j.cattod.2011.01.040

Rachiero, G. P., Demirci, U. B., and Miele, P. (2011b). Bimetallic RuCo and RuCu catalysts supported on γ-AlO. A comparative study of their activity in hydrolysis of ammonia-borane. *Int. J. Hydrogen Energy* 36, 7051–7065. doi: 10.1016/j.ijhydene.2011.03.009

Rakap, M., and Özkar, S. (2010). Zeolite confined palladium (0) nanoclusters as effective and reusable catalyst for hydrogen generation from the hydrolysis of ammonia-borane. *Int. J. Hydrogen Energy* 35, 1305–1312. doi: 10.1016/j.ijhydene.2009.11.056

Reber, A. C., Khanna, S. N., Roach, P. J., Woodward, W. H., and Castleman, A. W. (2010). Reactivity of aluminum cluster anions with water: origins of reactivity and mechanisms for H_2 release. *J. Phys. Chem. A* 114,6071–6081. doi: 10.1021/jp911136s

Roach, P. J., Woodward, W. H., Castleman, A. W., Reber, A. C., and Khanna, S. N. (2009). Complementary active sites cause size-selective reactivity of aluminum cluster anions with water. *Science* 323, 492–495. doi: 10.1126/science.1165884

Sanyal, U., Demirci, U. B., Jagirdar, B. R., and Miele, P. (2011). Hydrolysis of ammonia borane as a hydrogen source: fundamental issues and potential solutions towards implementation. *ChemSusChem.* 4, 1731–1739. doi: 10.1002/cssc.201100318

Shevlin, S. A., Kerkeni, B., and Guo, Z. X. (2011). Dehydrogenation mechanisms and thermodynamics of MNH_2BH_3 (M = Li, Na) metal amidoboranes as predicted from first principles. *Phys. Chem. Chem. Phys.* 13, 7649–1659. doi: 10.1039/c0cp02213f

Staubitz, A., Robertson, A. P. M., and Manners, I. (2010). Ammonia-Borane and related compounds as dihydrogen sources. *Chem. Rev.* 110, 4079–4124. doi: 10.1021/cr100088b

Stowe, A. C., Shaw, W. J., Linehan, J. C., Benjamin, S., and Autrey, T. (2007). In situ solid state ^{11}B MAS-NMR studies of the thermal decomposition of ammonia borane: mechanistic studies of the hydrogen release pathways from a solid state hydrogen storage material. *Phys. Chem. Chem. Phys.* 9, 1831–1836. doi: 10.1039/b617781f

Sun, D., Mazumder, V., Metin, O., and Sun, S. (2011). Catalytic hydrolysis of ammonia borane via cobalt palladium nanoparticles. *ACS Nano* 5, 6458–6464. doi: 10.1021/nn2016666

Thorne, L. R., Suenram, R. D., and Lovas, F. J. (2011). Microwave spectrum, torsional barrier, and structure of BH_3NH_3. *J. Chem. Phys.* 78, 167–171. doi: 10.1063/1.444528

Umegaki, T., Yan, J. M., Zhang, X. B., Shioyama, H., Kuriyama, N., and Xu,Q. (2009). Boron- and nitrogen-based chemical hydrogen storage materials. *Int. J. Hydrogen Energy* 34, 2303–2311. doi: 10.1016/j.ijhydene.2009.01.002

Wang, C. L., Tuninetti, J., Wang, Z., Zhang, C., Ciganda, R., Salmon, L., et al. (2017a). Hydrolysis of ammonia-borane over Ni/ZIF-8 nanocatalyst: high efficiency, mechanism, and controlled hydrogen release. *J. Am. Chem. Soc.* 139, 11610–11615. doi: 10.1021/jacs.7b06859

Wang, J., Qin, Y. L., Liu, X., and Zhang, X. B. (2012). *In situ* synthesis of magnetically recyclable graphene-supported Pd@Co coreshell nanoparticles as efficient catalysts for hydrolytic dehydrogenation of ammonia borane. *J. Mater. Chem.* 22, 12468–12470. doi: 10.1039/C2JM32229C

Wang, W. H., Tang, H. P., Lu, W. D., Li, Y., Bao, M., and Himeda, Y. (2017b). Mechanistic insights into the catalytic hydrolysis of ammonia borane with proton-responsive iridium complexes: an experimental and theoretical study. *ChemCatChem* 9, 3191–3196. doi: 10.1002/cctc.201700325

White, J. A., and Bird, D. M. (1994). Implementation of gradient-corrected exchange-correlation potentials in Car-Parrinello totalenergy calculations. *Phys. Rev. B* 50, 4954–4957. doi: 10.1103/PhysRevB.50.4954

Wu, Z., Xu, L., Zhang, W., Ma, Y., Yuan, Q., Jin, Y., et al. (2013). Structure sensitivity of low-temperature NO decomposition on Au surfaces. *J. Catal.* 304, 112–122. doi: 10.1016/j.jcat.2013.04.013

Xi, P., Chen, F., Xie, G., Ma, C., Liu, H., Shao, C., et al. (2012). Surfactant free RGO/Pd nanocomposites as highly active heterogeneous catalysts for the hydrolytic dehydrogenation of ammonia borane for chemical hydrogen storage. *Nanoscale* 4, 5597–5601. doi: 10.1039/c2nr31010d

Xu, Q., and Chandra, M. (2006). Catalytic activities of non-noble metals for hydrogen generation from aqueous ammonia-borane at room temperature. *J. Power Sources* 163, 364–370. doi: 10.1016/j.jpowsour.2006.09.043

Xu, Q., and Chandra, M. (2007). A portable hydrogen generation system: catalytic hydrolysis of ammonia-borane. *J. Alloy Compd.* 446, 729–732. doi: 10.1016/j.jallcom.2007.01.040

Yan, J. M., Zhang, X. B., Akita, T., Haruta, M., and Xu, Q. (2010a). One-step seeding growth of magnetically recyclable Au@Co core-shell nanoparticles: highly efficient catalyst for hydrolytic dehydrogenation of ammonia borane. *J. Am. Chem. Soc.* 132, 5326–5327. doi: 10.1021/ja910513h

Yan, J. M., Zhang, X. B., Han, S., Shioyama, H., and Xu, Q. (2008). Iron-nanoparticle-catalyzed hydrolytic dehydrogenation of ammonia borane for chemical hydrogen storage. *Angew. Chem. Int. Ed.* 47, 2287–2289. doi: 10.1002/anie.200704943

Yan, J. M., Zhang, X. B., Han, S., Shioyama, H., and Xu, Q. (2009). Synthesis of longtime water/air-stable Ni nanoparticles and their high catalytic activity for hydrolysis of ammoniaeborane for hydrogen generation. *Inorg. Chem.* 48, 7389–7393. doi: 10.1021/ic900921m

Yan, J. M., Zhang, X. B., Shioyama, H., and Xu, Q. (2010b). Room temperature hydrolytic dehydrogenation of ammonia borane catalyzed by Co nanoparticles. *J. Power Sources* 195, 1091–1094. doi: 10.1016/j.jpowsour.2009.08.067

Yao, C. F., Zhuang, L., Cao, Y. L., Ai, X. P., and Yang, H. X. (2008). Hydrogen release from hydrolysis of borazane on Pt-and Ni-based alloy catalysts. *Int. J. Hydrogen Energy* 3, 2462–2467. doi: 10.1016/j.ijhydene.2008.02.028

Zahmakiran, M., Durap, F., and Özkar, S. (2010). Zeolite confined copper (0) nanoclusters as cost-effective and reusable catalyst in hydrogen generation from the hydrolysis of ammonia-borane. *Int. J. Hydrogen Energy* 35, 187–197. doi: 10.1016/j.ijhydene.2009.10.055

Zahmakiran, M., and Özkar, S. (2009). Zeolite framework stabilized rhodium (0) nanoclusters catalyst for the hydrolysis of ammonia-borane in air: outstanding catalytic activity, reusability and lifetime. *Appl. Catal. B-Environ.* 89, 104–110. doi: 10.1016/j.apcatb.2008.12.004

Zhang, J., Li, H., Zhang, H., Zhu, Y., and Mi, G. (2016). Porously hierarchical Cu@Ni cubic-cage microstructure: Very active and durable catalyst for hydrolytically liberating H$_2$ gas from ammonia borane. *Renew. Energy* 99, 1038–1045. doi: 10.1016/j.renene.2016.07.066

Zhou, Q., Yang, H., and Xu, C. (2016). Nanoporous Ru as highly efficient catalyst for hydrolysis of ammonia borane. *Int. J. Hydrogen Energy* 41, 12714–12721. doi: 10.1016/j.ijhydene.2016.05.128

Zhou, T., Wang, G., Cui, H., Yuan, H., Kuang, A., Tian, C. L., et al. (2016). A novel dehydrogenation style of NH$_3$BH$_3$ by catalyst of transition metal clusters. *Int. J. Hydrogen Energy* 41, 11746–11760. doi: 10.1016/j.ijhydene.2015.12.201

Zins, E. L., Silvi, B., and Alikhani, M. E. (2015). Activation of C-H and B-H bonds through agostic bonding: an ELF/QTAIM insight. *Phys. Chem. Chem. Phys.* 17, 9258–9281. doi: 10.1039/C4CP05728G